Juan, Rongfei; Nguyen Xuan, Binh; Liu, Wenqi; Lian, Junhe

Optimizing crystal plasticity model parameters via machine learning-based optimization algorithms

Published in:
Material Forming: The 26th International ESAFORM Conference on Material Forming - ESAFORM 2023 - held in Kraków, Poland, April 19-21, 2023

DOI:
10.21741/9781644902479-153

Published: 01/01/2023

Document Version
Publisher's PDF, also known as Version of record

Materials Research Proceedings 28 (2023) 1417-1426 https://doi.org/10.21741/9781644902479-153

Optimizing crystal plasticity model parameters via machine learning-based optimization algorithms

JUAN Rongfei[1,a], BINH Nguyen Xuan[1,b], LIU Wenqi[1,c] and LIAN Junhe[1,d *]

[1]Advanced Manufacturing and Materials, Department of Mechanical Engineering, Aalto University, 02150 Espoo, Finland

[a]rongfei.juan@aalto.fi, [b] binh.nguyen@aalto.fi, [c] wenqi.liu@aalto.fi, [d] junhe.lian@aalto.fi

Keywords: Crystal Plasticity Model, Machine Learning, Parameter Calibration

Abstract. The field of materials science and engineering is constantly evolving, and new methods are being developed to improve our understanding of the relationship between microstructure and properties. One such method is crystal plasticity (CP) modeling, which is widely used for predicting the mechanical properties of crystals and phases. However, determining the constitutive parameters for CP models has been a significant challenge, with current methods relying on either direct chemical composition or inverse fitting, both of which can be time-consuming and lack accuracy. In this study, we propose an automated, advanced, and more efficient method for determining constitutive parameters by using a genetic algorithm (GA) optimization method coupled with machine learning. Our proposed method is applied to two widely used CP models, and the reference data for the calibration is the stress-strain curve from tensile tests. The results of the automated calibration process are then compared to numerical simulation results of CP models with known parameters, demonstrating the efficiency and accuracy of our proposed method.

Introduction

In the field of materials science and engineering, the integrated computational materials and engineering (ICME) approach provides a comprehensive and quantifiable description of the relationship between microstructure and properties. One such approach is crystal plasticity (CP) modeling, which is widely employed for predicting the crystal and phase-level mechanical properties of materials. The CP model has been successfully used to predict the number of ears formed during the cupping process, the anisotropic deformation behavior, the yield locus, the hardening curves, and the residual stress formation during deformation. Currently, there are two prominent crystal plasticity constitutive laws: the phenomenological (PH) and the dislocation-based (DB) constitutive laws. These laws diverge in explaining the dislocation evolution and the interaction laws between slip planes at the microscopic level [1]. In other words, the two laws define the strain-hardening process differently with their own set of equations and resultant fitting parameters. Both constitutive laws aim to define the kinetic equation for the shear rate $\dot{\gamma}$ on the slip system α. The phenomenological law defines the shear rate formula through empirical observation [2], while the law based on dislocation density derives the shear rate from physical kinetic equations that depend on material properties [3, 4].

Previous studies have used these two CP models to predict different types of nonlinear loading deformation with varying success [5-9]. However, the process of determining the constitutive parameters for CP models has been a significant challenge, with current methods relying on either direct chemical composition [10,11], which may lack a certain level of accuracy for specific applications, or inverse fitting of fitting constitutive parameters via a manual procedure that relies on the researcher's experience and is highly subjective and time-consuming.

In light of these challenges, several recent studies attempted to determine the optimal constitutive parameters by different optimization algorithms[12,13]. It is shown that the optimization algorithms, e.g., genetic algorithm (GA), could provide very accurate parameter

calibration for both models. However, the procedure to use the GA for the optimization process of CP models is not straightforward and a manual process shall be involved in formulating an empirical function serving as the response surface to save the computational time for GA.

Therefore, in the current study, it is aimed to formulate an automated, advanced, and more efficient method for determining constitutive parameters by using the GA optimization method. The main focus is to improve the efficiency and simplify the formulation of the response surface that is needed in the GA optimization process. A machine-learning-based approach is proposed for this purpose to be coupled with GA. The new method is applied to both CP models: four fitting parameters ($\tau_0, \alpha, h_0, \tau_{sat}$) in the phenomenological law and six fitting parameters ($\hat{d}^{\alpha}$, i_{slip}, Ω, p, q, τ_{sol}) in the dislocation-density-based law [5,9]. The reference data for the calibration is the stress-strain curve from tensile tests, which is also the most used case for single-phase materials [14]. In the study, numerical simulation results of CP models with known parameters are used as the target or "experimental" curve, which can be used to verify and compare the results of the parameters by the automated calibration process.

Methodology

The response surface methodology (RSM) is a frequently used mathematical model to analyze the response of interest [15]. RSM aims to accurately predict the response variables given an unknown set of explanatory variables. For example, in CP parameter calibration, the explanatory variables are the fitting parameters (four in PH law and six in DB law) and the response variables are the corresponding stress values. Therefore, the essential aspect of RSM is the true reflection of regional continuity around the global optima. This study uses the multilayer perceptron (MLP) as the RSM for the genetic algorithms. An MLP is a feedforward artificial neural network comprising an input layer, several hidden layers, and an output layer. The MLP structure used in this project consists of three layers: the input layer (parameters) with 4-6 neurons and the output layer (stress values) with varying neurons depending on the number of interpolated stress values. There is only one hidden layer, and the number of nodes in the hidden layer is calculated as:

$$N_{hidden} = round(\frac{2}{3} N_{input} + N_{output}) \quad (1)$$

The approximation depends on the hidden layer, where each neuron is the weighted linear sum of the neurons in the previous layer or the input layer. The output layer derives from the transformation of the hidden layer by the activation function, whose outputs depend on whether the inputs pass their respective thresholds. Rectified Linear Unit (ReLU) is used as the activation function for its common usage and exemplary performance in neural networks:

$$\text{ReLU}(x) = max(x, 0) \quad (2)$$

where x is the value in the hidden nodes. The function returns 0 if x is negative.

Optimization of complex functions with unknown structures is a challenging problem to solve. The genetic algorithm, a commonly used hyperparameter optimization algorithm, is applied in this research to tackle this problem. This algorithm is based on the theory of evolution by Charles Darwin, where survival of the fittest is regarded as the best outcome. A study by Himani Panwar [16] finds that the natural selection process is simulated by choosing the best individuals 11 from each generation determined by the fitness function. According to Sedighiani [12], GA can converge to the global optimum of the objective functions instead of being stuck in local optima like the gradient-based searching methods. For this reason, GA is a robust optimization algorithm that guarantees to find the optimal solution in a probabilistic fashion of biological evolution.

Fig. 1 shows the structure of GA is mainly based on the work of Sedighiani et al. [12], which features eight steps that simulate biological evolution. The goal of GA is to maximize the fitness functions in one iteration.

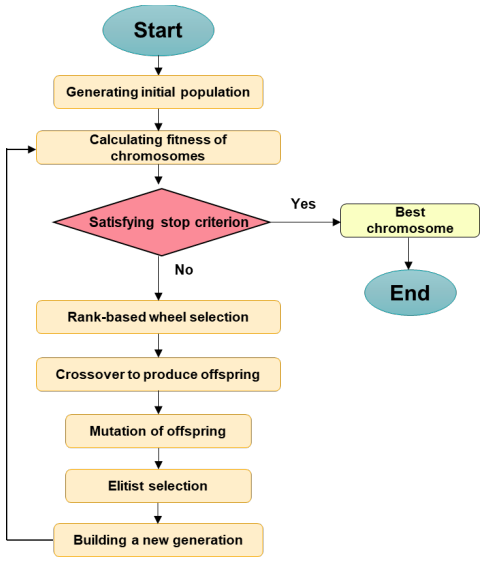

Fig. 1. GA workflow comparison in each iteration.

Objective, Fitness, and Stop Criteria Functions

In this study, a multi-objective optimization approach was developed to improve the precision of simulation results. The optimization process was divided into two stages, with the first stage focusing on optimizing the parameters that control yield strength and the second stage focusing on optimizing the parameters that control hardening behavior.

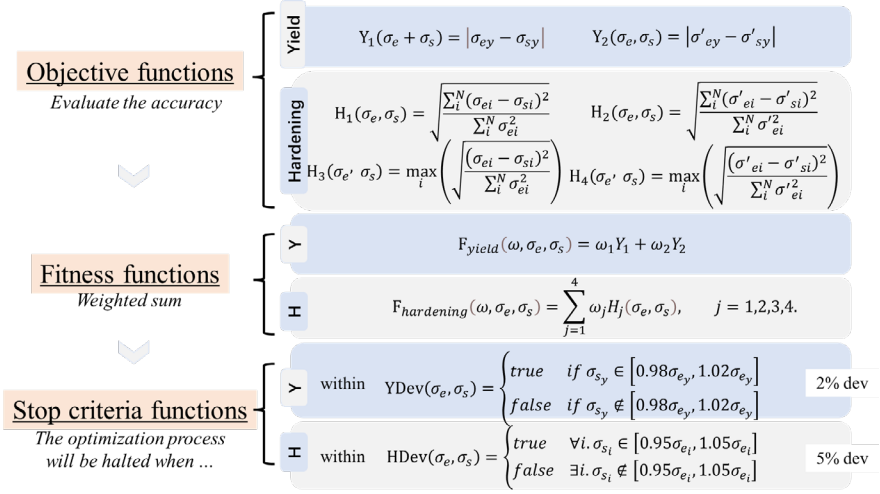

Fig. 2. Overview of the multi-objective optimization approach functions.

Fig. 2 shows all the functions of the optimization, which are the objective, fitness, and stop criteria functions. In the first stage of optimization, two objective functions were employed to evaluate the accuracy of simulated yield strength. The first objective function, Y_1, measured the absolute difference between the experimental and simulated yield strength values, while the second objective function, Y_2, calculated the slope of yield strength.

$$Y_1(\sigma_e,\sigma_s)=|\sigma_{ey}-\sigma_{sy}| \tag{3}$$

$$Y_2(\sigma_e, \sigma_s) = \left|\sigma'_{ey} - \sigma'_{sy}\right| \quad (4)$$

where σ_{ey} and σ_{sy} are the yield strength of the experiment and simulation curves, and σ'_{ey} and σ'_{sy} are the slope of the yield strength of experiments and simulation, respectively. As shown in the fitness function later, a linear combination of these two objective functions, Y1 and Y2, was used to minimize the deviation between the experimental and simulated yield strength values, as well as the deviation in the slope of the yield strength. This approach helped to quantify the yield strength accuracy more precisely and take into account the increasing trend of the experimental and simulated yield strength.

In the second stage of optimization, four objective functions were utilized to evaluate the global fitness of the simulated hardening behavior. The first objective function measured the normalized Euclidean distance between the experimental and simulated hardening curves, while the second objective function measured the normalized slope difference between the two curves. This helped to determine whether the simulated and experimental hardening curves shared the same global shape.

$$H_1(\sigma_e, \sigma_s) = \sqrt{\frac{\sum_i^N (\sigma_{ei} - \sigma_{si})^2}{\sum_i^N \sigma_{ei}^2}} \quad (5)$$

$$H_2(\sigma_e, \sigma_s) = \sqrt{\frac{\sum_i^N (\sigma'_{ei} - \sigma'_{si})^2}{\sum_i^N \sigma'^2_{ei}}} \quad (6)$$

In the two objective functions, the subscript *i* stand for each data point in the hardening part of the stress–strain curves for both experiments and simulations, and *N* represents the total number of data points.

To further penalize the maximum distance and slope difference between the curves, two additional objective functions, H_3 and H_4, were employed which delivered the maximum value point of H_1 and H_2, respectively. These objective functions helped to account for the maximum deviation and slope difference between the experimental and simulated curves. A linear combination of these four objective functions was used to converge to the global optimum and avoid getting stuck in local optima.

$$H_3(\sigma_e, \sigma_s) = \max_i \left(\sqrt{\frac{(\sigma_{ei} - \sigma_{si})^2}{\sum_i^N \sigma_{ei}^2}} \right) \quad (7)$$

$$H_4(\sigma_e, \sigma_s) = \max_i \left(\sqrt{\frac{(\sigma'_{ei} - \sigma'_{si})^2}{\sum_i^N \sigma'^2_{ei}}} \right) \quad (8)$$

The fitness function for each optimization stage was the weighted sum of all objective functions. In the first stage, the yield stress fitness function was the weighted sum of Y_1 and Y_2, while the hardening fitness function in the second stage was the weighted sum of the hardening objective functions. The weights could be manually tuned to improve the results in each stage when certain fitness aspects required emphasis. The sum of the weights was defined to be one, with the difference in the weights being due to the unequal importance and result scale of the objective functions.

$$F_{yield}(\omega, \sigma_e, \sigma_s) = \omega_1 Y_1 + \omega_2 Y_2 \quad (9)$$

$$F_{hardening}(\omega, \sigma_e, \sigma_s) = \sum_{j=1}^{4} \omega_j H_j(\sigma_e, \sigma_s), \; j = 1,2,3,4 \quad (10)$$

The optimization process was halted when the stopping criteria were met. In the first stage, the process stopped when the simulated yield strength value was within a specified deviation from the experimental value, as defined in YDev. A rather small tolerance, 2% is chosen for this case to ensure very good fitness on the yield strength. In the second stage, the process stopped when all simulated stress values were within a specified deviation, 5%, of the experimental stress values, as defined in the HDev function. These stopping criteria ensured that the final simulation results met the desired precision and accuracy.

$$\mathrm{YDev}(\sigma_e,\ \sigma_s) = \begin{cases} true & if\ \sigma_{s_y} \in \left[0.98\sigma_{e_y},\ 1.02\sigma_{e_y}\right] \\ false & if\ \sigma_{s_y} \notin \left[0.98\sigma_{e_y},\ 1.02\sigma_{e_y}\right] \end{cases} \tag{11}$$

$$\mathrm{HDev}(\sigma_e,\ \sigma_s) = \begin{cases} true & \forall i.\ \sigma_{s_i} \in \left[0.95\sigma_{e_i},\ 1.05\sigma_{e_i}\right] \\ false & \exists i.\ \sigma_{s_i} \notin \left[0.95\sigma_{e_i},\ 1.05\sigma_{e_i}\right] \end{cases} \tag{12}$$

Experimental and simulated data were used in this process and precise yield stress values and similar global shapes to the target curves were obtained, which will be shown in the next section. In Table 1, the default weights for the fitness functions used in this study are shown. The developed optimization approach was effective in improving the precision of simulation results and could be applied to various optimization problems in the field. Additionally, the approach allowed for manual tuning of the weights for the objective functions to emphasize specific aspects of the fitness, providing more flexibility in the optimization process.

Table 1. Default weights for two fitness functions.

	F_{yield}		$F_{hardening}$			
	ω_{y1}	ω_{y2}	ω_{h1}	ω_{h1}	ω_{h1}	ω_{h1}
weight	0.999	0.001	0.9	0.025	0.05	0.025

Resutls and Discussion

Before the optimization, we must ensure our target curve and search space for the optimizer. Instead of the experimental data, the target strain-stress curves are taken from the CP simulation for a better comparison of the quality of the fitted parameters by the optimization approach. To prove the general validity of the proposed approach for different types of materials, not only one simulation but three simulation results with very different parameter sets were selected as the target curves to compare the difference between the initial parameter values with the optimal parameters delivered by the calibration process. Next, we need to determine the parameter ranges and step sizes. The range allows the optimizer to limit the search space, and the step size allows for the discretization of continuous parameter values. Therefore, the algorithms only search within the range by the defined step size.

The CP model calibration process begins with converting the true stress-true strain curve into the flow curve in the preprocessing stage. Next, initial simulations are performed, which will yield the final optimal parameters that are dependent on the parameters of the initial simulations. Good initial simulations help direct the optimizing algorithm to the location of the true parameter set. The number of initial simulations in this work is 30. To improve the precision of both yield stress and hardening parameter predictions, the range of all simulated yield stresses must cover the experimental yield stress and the boundaries should cover the experimental global curve. Additionally, the neighboring simulated curves should have a similar global shape to that of the target curve. Fig. 3 shows the relationship between the initial guess simulations and target curves.

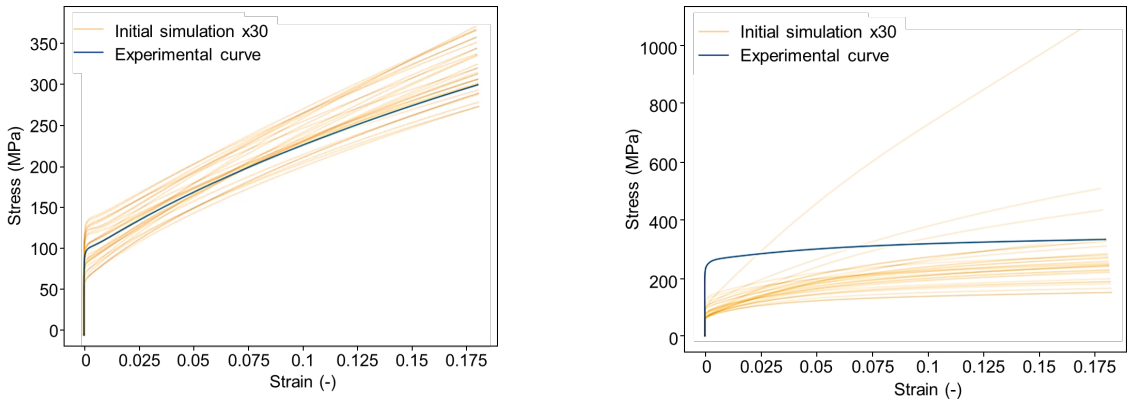

(a) Good initial simulations (b) Bad initial simulations

Fig. 3. Good (a) and bad (b) initial simulations and experimental curve.

The first stage of the optimization process involves adjusting the yield stress parameters, which are represented by τ_0 for the PH model and p, q, and τ_{sol} for the DB model. The hardening parameters are not altered during this stage. The results of this stage are illustrated in Fig. 4a for the PH model, where it can be observed that in the first iteration, the simulated yield stress (σ_{sy}) is approximately 123.5 MPa at $\tau_0 = 52$. In the following iteration, the genetic algorithm predicts $\tau_0 = 51$, resulting in a further increase in σsy. The optimization process concludes in the third iteration, where $\tau_0 = 54$ and σsy deviates by 2% from the experimental yield stress (σ_{ey}) whose true value is $\tau_0 = 55$. It is important to note that the algorithm does not always produce better results in each iteration; instead, it demonstrates an improvement trend, with simulated yield stress values progressively approaching the experimental yield stress. This is because the algorithm explores different parts of the search space in each iteration, gradually honing in on the true parameter set. Similarly, for the DB model, the optimized parameters are (p, q, τ_{sol}) = (0.2, 1.3, 0.3), which results in a 2% deviation in the yield stress from the true parameters (p, q, τ_{sol}) = (0.2, 1.8, 0.4) as shown in Fig. 4b. Despite not being exact, the results are still satisfactory due to the non-uniqueness of optimal parameters. This means that even if one parameter is changed, another varying parameter can exist to balance the outcome.

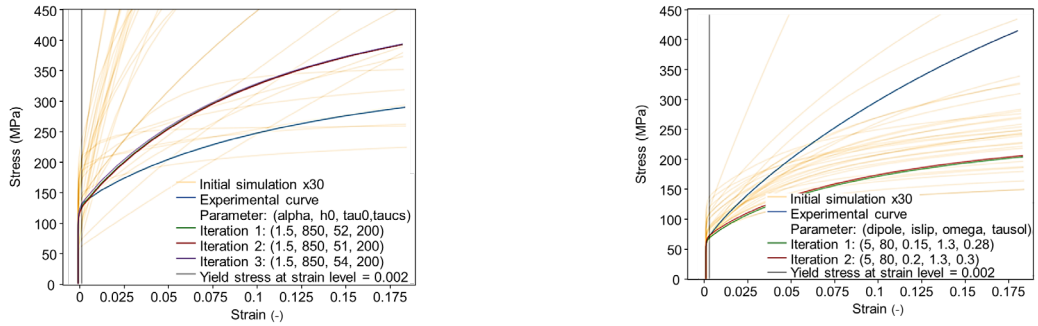

(a) Yield control optimized by GA of PH (b) Yield control optimized by GA of DB

Fig. 4 Strain-stress curve of σ_y at $\varepsilon = 0.002$ in the first optimize stage of PH (a) and DB (b).

In the second stage of the optimization process, the algorithms focus on adjusting the hardening parameters. For the PH model, these parameters are represented by α, h_0, and τ_{sat}, while for the DB model, they are represented by $\hat{d}^{\alpha}$, i_{slip}, and Ω. The values of the yield stress adjusting parameters are obtained from the first stage of the optimization process. The results of this stage are illustrated in Fig. 5 for both the PH and DB models.

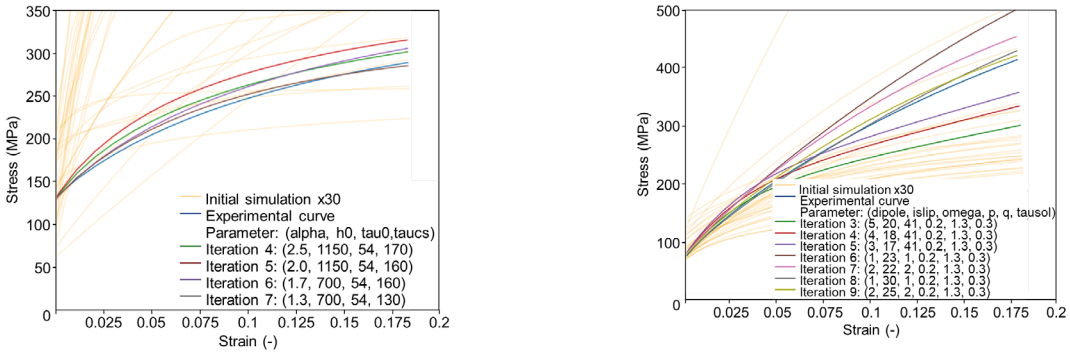

(b) Hardening behavior optimization of PH (b) Hardening behavior optimization of DB

Fig. 5 Strain-stress curve in the second optimization stage of PH (a) and DB (b).

The quality of the fitting simulation curve is evaluated based on two criteria: the loss distance and the number of intersections with the experimental curve. The goal is to achieve a minimum distance loss and to have the simulated curve globally above, below, or exactly overlapping the experimental curve. This is because these conditions indicate that the simulated and experimental curves share the same increasing trend, which is a good indication of the accuracy of the simulation. On the other hand, if the simulated curve intersects with the experimental curve, it indicates contrasting material performance and a loss of the simulated prediction meaning. In the last iteration (7th) of the PH1 model, the simulated curve shares two intersections with the experimental curve, while in the DB1 model, the last iteration (9th) shares no intersections, making the final simulation result of DB1 better than PH1 in terms of the above-mentioned criteria.

Following the procedures demonstrated above, the performance of the final iteration results of the parameter calibration program under GA was then compared and illustrated in Fig. 6. The GA demonstrates good and stable calibration quality for the three initial target curves of both the PH and DB model. Similar conclusions were also observed in the results of the DB laws. Table 2 below records all optimal parameter solutions predicted by GA. It is important to note that in some cases, more than one parameter controls the same aspect of the simulation, and their effects can balance each other out. For example, only τ_0 controls the yield point of PH, while other parameters control the hardening curve, and a and h_0 have opposite effects on the hardening curve.

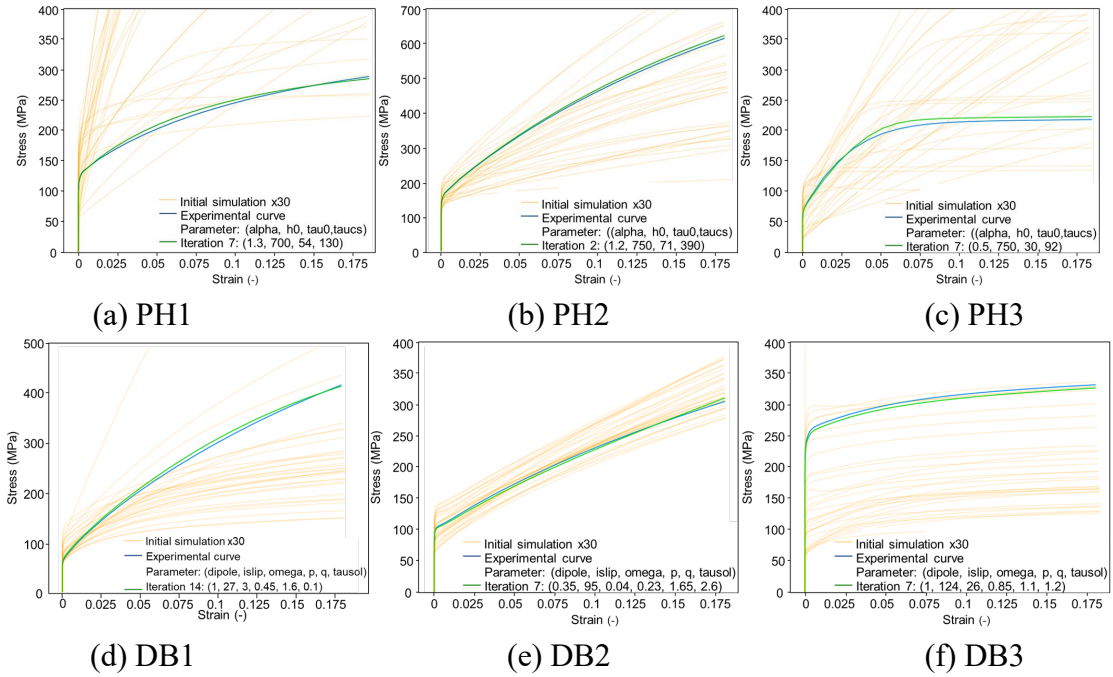

(a) PH1 (b) PH2 (c) PH3

(d) DB1 (e) DB2 (f) DB3

Fig. 6. Final iteration of parameter calibration for target curves in PH and DB laws.

Table 2. Final fitting parameter calibration results for two CP models.

	τ_0	a	h_0	τ_{sat}		$\hat{d}^{\alpha}$	i_{slip}	Ω	p	q	τ_{sol}
PH1	54	1.3	700	130	DB1	1	27	3	0.45	1.6	0.10
True	55	1.6	600	150	True	1	25	3	0.20	1.8	0.40
PH2	71	1.2	750	390	DB2	0.35	95	0.04	0.23	1.65	2.60
True	70	1.9	800	500	True	0.80	80	0.80	0.20	1.10	1.20
PH3	30	0.5	750	92	DB3	2	140	10	0.85	1.10	1.20
True	30	0.8	1000	90	True	2	180	15	0.90	1.10	1.20

Fig. 7 shows the comparison of the yield point error and the root means square error (RSME) of the hardening behavior between experimental data and optimized results. As seen in Fig. 7a, the error analysis of GA at the yield point shows relatively small values, within a 2% deviation from the experimental ones. Meanwhile, in Fig. 7b, the RSME values for the hardening behavior also indicate that the fitting quality for the three cases shows very good quality.

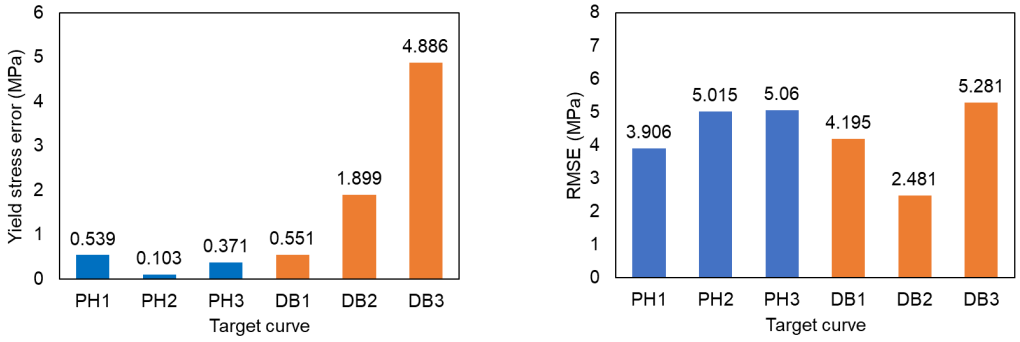

(a) Yield stress error comparison (b) Root mean square error comparison

Fig. 7. Error analysis of the final iteration of parameter calibration for the three target curves.

Summary

The optimization workflow presented in this study solves well the problem of parameter calibration for three chosen target stress-strain curves, which traditionally relies on educated

guessing by experts. Additionally, the use of machine learning-assisted methodology in this article has led to a fully automated process for identifying fitting parameters. Despite the success of the calibration process in identifying optimal fitting parameters, certain challenges and limitations also exist in the current workflow. These include:

- Choosing an appropriate parameter range: If the true parameters do not lie within the specified range, the optimization algorithm may not converge to the correct solution unless the optimal solution is non-unique and another candidate within the range behaves similarly to the target curve.
- Poor initial simulations: Initial simulations should be regenerated when the yield stress is not covered in the range of simulated yield stress values.
- Nonconvergence of simulations in the DB model: Not all combinations of DB fitting parameters result in successfully converging simulations. This problem usually arises from large $\hat{d}^{\alpha}$ and very small p values.
- Nonconvergence of the MLP regressor: This issue can occur due to a large number of data points in the target curve and can be solved by loading point interval omission.

These limitations and challenges present in the current workflow can be overcome by certain adjustments, such as adjusting the chosen parameters, and are currently being solved in a more general and automated matter in ongoing studies.

Acknowledgments
Simulations were performed with computing resources granted by the Finnish IT Center for Science (CSC) services. The authors gratefully acknowledge CSC [project number: 2004956 Optimization of crystal plasticity parameter calibration] for the simulation resources for the project. All the authors also are grateful to Ilari Pajula, Nam Anh Chu, and Lucas Krieger from group 1 of the Computational Engineering project course at Aalto University for preliminary work and related discussion on this study.

References
[1] F. Roters, M. Diehl, P. Shanthraj, P. Eisenlohr, C. Reuber, S.L. Wong, T. Maiti, A. Ebrahimi, T. Hochrainer, H.O. Fabritius, S. Nikolov, M. Friak, N. Fujita, N. Grilli, K.G.F. Janssens, N. Jia, P.J.J. Kok, D. Ma, F. Meier, E. Werner, M. Stricker, D. Weygand, D. Raabe, DAMASK - The Dusseldorf Advanced Material Simulation Kit for modeling multi-physics crystal plasticity, thermal, and damage phenomena from the single crystal up to the component scale, Computat. Mater. Sci. 158 (2019) 420-478. https://doi.org/10.1016/j.commatsci.2018.04.030
[2] E. Voce, The Relationship between Stress and Strain for Homogeneous Deformation, J. I. Met. 74 (1948) 537-562.
[3] S.L. Wong, M. Madivala, U. Prahl, F. Roters, D. Raabe, A crystal plasticity model for twinning- and transformation-induced plasticity, Acta Mater. 118 (2016) 140-151. https://doi.org/10.1016/j.actamat.2016.07.032
[4] F.J. Gallardo-Basile, Y. Naunheim, F. Roters, M. Diehl, Lath Martensite Microstructure Modeling: A High-Resolution Crystal Plasticity Simulation Study, Materials 14 (2021) 691. https://doi.org/10.3390/ma14030691
[5] R. Juan, W. Liu, X. Inza, X. Ureta, J. Mendiguren, J. Lian, Crystal Plasticity Modeling of Al Alloy under Linear and Non-Linear Loading, Key Eng. Mater. 926 (2022) 2099-2108. http://doi.org/10.4028/p-2jqp1v
[6] J. Lian, W. Liu, X. Gastañares, R. Juan, J. Mendiguren, Plasticity evolution of an aluminum-magnesium alloy under abrupt strain path changes, Int. J. Mater. Form. 15 (2022) 40. https://doi.org/10.1007/s12289-022-01692-6

[7] M. Bertin, C.W. Du, J.P.M. Hoefnagels, F. Hild, Crystal plasticity parameter identification with 3D measurements and Integrated Digital Image Correlation, Acta Mater. 116 (2016) 321-331. https://doi.org/10.1016/j.actamat.2016.06.039
[8] D. Raabe, M. Sachtleber, Z. Zhao, F. Roters, S. Zaefferer, Micromechanical and macromechanical effects in grain scale polycrystal plasticity experimentation and simulation, Acta Mater. 49 (2001) 3433-3441. https://doi.org/10.1016/S1359-6454(01)00242-7
[9] W. Liu, J. Lian, N. Aravas, S. Münstermann, A strategy for synthetic microstructure generation and crystal plasticity parameter calibration of fine-grain-structured dual-phase steel, Int. J. Plast. 126 (2020) 102614. https://doi.org/10.1016/j.ijplas.2019.10.002
[10] C.C. Tasan, J.P.M. Hoefnagels, M. Diehl, D. Yan, F. Roters, D. Raabe, Strain localization and damage in dual phase steels investigated by coupled in-situ deformation experiments and crystal plasticity simulations, Int. J. Plast. 63 (2014) 198-210. http://doi.org/10.1016/j.ijplas.2014.06.004
[11] H.J. Bong, H. Lim, M.-G. Lee, D.T. Fullwood, E.R. Homer, R.H. Wagoner, An RVE procedure for micromechanical prediction of mechanical behavior of dual-phase steel, Mater. Sci. Eng. A 695 (2017) 101-111. https://doi.org/10.1016/j.msea.2017.04.032
[12] K. Sedighiani, M. Diehl, K. Traka, F. Roters, J. Sietsma, D. Raabe, An efficient and robust approach to determine material parameters of crystal plasticity constitutive laws from macro-scale stress-strain curves, Int. J. Plast. 134 (2020) 102779. https://doi.org/10.1016/j.ijplas.2020.102779
[13] J. Kuhn, J. Spitz, P. Sonnweber-Ribic, M. Schneider, T. Bohlke, Identifying material parameters in crystal plasticity by Bayesian optimization, Optim. Eng. 23 (2022) 1489-1523. https://doi.org/10.1007/s11081-021-09663-7
[14] K. Zhang, B. Holmedal, S. Hopperstad, S. Dumoulin, J. Gawad, A. Van Bael, P. Van Houtte, Multi-level modelling of mechanical anisotropy of commercial pure aluminium plate: Crystal plasticity models, advanced yield functions and parameter identification, Int. J. Plast. 66 (2015) 3-30. https://doi.org/10.1016/j.ijplas.2014.02.003
[15] D.T. Do, D.H. Lam, T. Nguyen, T.T. Phuong Mai, L.T.M. Phan, H.T. Vuong, D.V. Nguyen, N.T.T. Linh, M.N. Hoang, T.P. Mai, H.H. Nguyen, Utilization of Response Surface Methodology in Optimization of Polysaccharides Extraction from Vietnamese Red Ganoderma lucidum by Ultrasound-Assisted Enzymatic Method and Examination of Bioactivities of the Extract, Scientific World Journal 2021 (2021) 7594092. https://doi.org/10.1155/2021/7594092
[16] P. Himani Panwar, Dharamveer Singh, Abha Singh, Genetic Algorithm for Solving Simple Mathematical Equality Problem, IRJET 07 (2020) 7622-7627.